Journal of the Physical Society of Japan **84**, 064713 (2015)
http://dx.doi.org/10.7566/JPSJ.84.064713

Tunneling Spectroscopy in Organic Superconductor κ-(BEDT-TTF-d[3,3])$_2$Cu[N(CN)$_2$]Br

Yuki Oka[1], Hiroyoshi Nobukane[1], Noriaki Matsunaga[1], Kazushige Nomura[1], Kazuhiro Katono[2], Koichi Ichimura[2], and Atsushi Kawamoto[1]

[1]*Department of Physics, Hokkaido University, Sapporo 060-0810, Japan*
[2]*Department of Applied Physics, Hokkaido University, Sapporo 060-8628, Japan*

(Received January 27, 2015; accepted April 9, 2015; published online May 26, 2015)

We performed tunneling spectroscopy (STS) measurement in an organic superconductor, partially deuterated κ-(BEDT-TTF-d[3,3])$_2$Cu[N(CN)$_2$]Br. We carried out angle-resolved STS on cut lateral surfaces by the focused ion beam (FIB) method as well as as-grown single-crystal surfaces. It was found that the d[3,3]-Br salt is a strong-coupling *d*-wave superconductor and that the nodal direction is at an angle of $\pi/4$ from the a^*-axis, corresponding to the $d_{x^2-y^2}$ symmetry in the bulk superconducting phase. It is understood that the electron correlation in the d[3,3]-Br salt is not strong enough on the basis of the spin fluctuation mechanism. On the other hand, we also observed two types of superconducting gap. This suggests the coexistence of the $d_{x^2-y^2}$ and d_{xy} symmetries. This indicates a change in the symmetry from $d_{x^2-y^2}$ in the bulk superconducting phase to d_{xy} around the insulating region with increasing electron correlation.

1. Introduction

A salt of κ-(BEDT-TTF)$_2X$ is a quasi-two-dimensional organic conductor and its band filling is considered to be the half-filled because of the strong dimerization of the BEDT-TTF (ET) molecules. These κ-ET salts show some different electronic ground states such as the superconducting and magnetic Mott insulating states, depending on the effective pressure. Their overall behaviors are well summarized in a phase diagram with the ratio of the electron correlation to the bandwidth $U_{\rm eff}/W$, where $U_{\rm eff}$ is the effective on-site Coulomb energy on the ET dimer and W is the bandwidth, corresponding to the pressure.[1)] In this dimer system, the magnitude of $U_{\rm eff}$ is dominated by the degree of dimerization of the ET molecules as described by $U_{\rm eff} = 2t_{\rm dimer}$, where $t_{\rm dimer}$ is the intradimer transfer integral.[2)] A decrease in the pressure causes an increase in $U_{\rm eff}/W$ through an increase in $t_{\rm dimer}$. In the phase diagram, κ-(ET)$_2$Cu(NCS)$_2$ and κ-(ET)$_2$Cu[N(CN)$_2$]Br are located in the higher-pressure region and show superconductivity at 10.4 and 11.6 K, respectively. The superconducting transition temperature $T_{\rm c}$ increases slightly from the Cu(NCS)$_2$ salt to the Cu[N(CN)$_2$]Br salt with increasing electron correlation towards the Mott boundary. On the other hand, κ-(ET)$_2$Cu[N(CN)$_2$]Cl, which is located in the lower-pressure region than the Cu[N(CN)$_2$]Br salt, shows an antiferromagnetic insulating transition below 30 K[3)] at ambient pressure. This salt also shows superconductivity at approximately 13 K above a pressure of 30 MPa. Furthermore, the magnitude of $U_{\rm eff}$ can also be controlled finely near the Mott boundary by deuteration of the ethylene groups of the ET molecule.[4)] The d[0,0]-Cu[N(CN)$_2$]Br salt (n in d[n,n]-Br means the number of ethylene groups of the ET molecule substituted by deuterium) undergoes the superconducting transition, while the d[4,4]-Br salt lies on the Mott boundary and shows antiferromagnetic insulating behavior at the ground state. The enhancement of $(T_1T)^{-1}$ in ^{13}C-NMR[5)] from 200 to 60 K associated with the antiferromagnetic spin fluctuation has been observed even in the Cu[N(CN)$_2$]Br salt with the superconducting ground state, similarly to the case of the Cu[N(CN)$_2$]Cl salt with the antiferromagnetic insulating state. Its behaviors indicate that the magnitude of the electron correlation plays an important role in the relationship between the superconducting and Mott insulating states. Therefore, the attractive interaction between the electron pair mediated by the antiferromagnetic spin fluctuation is a strong candidate for the mechanism of its superconductivity.

There have been some investigations of the pairing mechanism of superconductivity in κ-ET salts, and the possibility of unconventional superconductivity different from BCS superconductivity has been discussed. The upper critical magnetic field $H_{\rm c2}$ of κ-(ET)$_2$Cu[N(CN)$_2$]Br parallel to the a–c conducting plane was determined as 30.6 T,[6)] larger than that of the Pauli limit (21.5 T). Although this result suggested spin-triplet electron pairing at a glance, the possibility of spin-singlet electron pairing cannot be denied since the Pauli limit value is likely to be enhanced by the effect of the larger spin–orbit interaction. Meanwhile, the Knight shift in ^{13}C-NMR[7,8)] decreases to zero well below $T_{\rm c}$. This decrease in the spin susceptibility unambiguously proves that the electron pairing in κ-ET salts is spin-singlet. The electronic specific heat of the Cu(NCS)$_2$ and Cu[N(CN)$_2$]Br salts shows not thermal activation dependence but power-law T^2-dependence at temperatures below $T_{\rm c}$.[9,10)] These results indicate probably *d*-wave superconductivity with nodes.

To investigate the superconducting gap symmetry, tunneling spectroscopy (STS) measurement using a scanning tunneling microscope (STM) is useful since the electronic density of states can be obtained directly with high energy resolution and less disturbance. In particular, angle-resolved STS measurement enables us to investigate the in-plane anisotropy of the superconducting gap in detail. The superconducting gap symmetry in the Cu(NCS)$_2$ salt was investigated by angle-resolved STS[11)] for the first time. Its result showed that the superconducting gap of the Cu(NCS)$_2$ salt has an anisotropic *d*-wave symmetry with the nodal direction at an angle of $\pi/4$ from the in-plane (b–c plane) wavenumber $\boldsymbol{k}$-axis, as described by the $d_{x^2-y^2}$ symmetry. The symmetry of the *d*-wave superconductivity was also investigated by thermal conductivity measurement in the Cu(NCS)$_2$ salt under a magnetic field rotated within the b–c

conducting plane. The field angular dependence of the thermal conductivity has fourfold symmetry and suggests the $d_{x^2-y^2}$ symmetry, similarly to the result of STS. This $d_{x^2-y^2}$ symmetry is not expected in a simple spin fluctuation mechanism such as cuprate superconductors. On the other hand, it has been predicted from a theoretical study[12] of the spin fluctuation mechanism considering the four electronic bands in the κ-ET salts that the nodal direction of the d-wave changes from the $d_{x^2-y^2}$ symmetry to the d_{xy} symmetry with increasing electron correlation. Accordingly, the results obtained from the angle-resolved STS and thermal conductivity measurements suggest that the electron correlation of the $Cu(NCS)_2$ salt is weak in the framework of this spin fluctuation model.

To investigate the relationship between the symmetry of the superconductivity and the electron correlation predicted by the spin fluctuation model in more detail, the gap symmetry was investigated for the d[0,0]-Br[13] and d[2,2]-Br[14] salts, which are situated nearer the Mott boundary than the $Cu(NCS)_2$ salt, by angle-resolved STS. The results indicate that the superconducting gap of these salts is also described by the $d_{x^2-y^2}$ symmetry, similarly to the $Cu(NCS)_2$ salt. The zero bias conductance peak (ZBCP) observed by STS is also an important feature of an anisotropic superconductor.[15] It is known that the ZBCP is observed in the case of gapless superconductivity, such as d-wave superconductivity with line nodes. In fact, the observation of the ZBCP has been reported for cuprates such as $YBa_2Cu_3O_{7-\delta}$,[15] $Bi_2Sr_2CaCu_2O_8$,[16] and $La_{2-\delta}Sr_\delta Cu_4O_{7-\delta}$.[17] The ZBCP was observed at the lateral surface in the d[0,0]-Br and d[2,2]-Br salts near the nodal direction, which is also consistent with the $d_{x^2-y^2}$ symmetry in these salts.[13,14] These facts mean that the electron correlation is not strong enough even in the d[2,2]-Br salt according to the spin fluctuation model.

From the above, it is important to investigate the superconducting gap symmetry in another κ-ET salt located very near the Mott boundary, such as the d[3,3]-Br salt, to clarify the mechanism of its superconductivity. In the d[3,3]-Br salt, we have already measured the superconducting gap on the conducting plane and the lateral surface by STS.[11,13,14] It was suggested that the superconducting gap symmetry is consistent with the $d_{x^2-y^2}$ symmetry, similarly to other previously studied κ-ET salts. However, we could not determine the nodal direction definitely because of the insufficient number of data points corresponding to surfaces of various directions owing to the single-crystal shape in the case of the as-grown crystal surface. For the accurate determination of the in-plane gap anisotropy, it is very important to perform angle-resolved STS at surfaces of various directions. In order to resolve this problem, we tried to cut the lateral surface perpendicular to the conducting plane at various angles using a focused ion beam (FIB) system and carried out angle-resolved STS at the FIB-cut surfaces.

In this article, we report the results of angle-resolved STS on as-grown and FIB-cut lateral surfaces in the d[3,3]-Br salt and discuss the mechanism of its superconductivity.

2. Experimental Procedure

Single crystals were grown by the standard electrochemical method.[18] The typical size was about $1 \times 1 \times 0.3$ mm^3. The directions of the lateral surface were determined by single-crystal X-ray structure analysis after STS measurement, and it was confirmed that the used samples are single crystals. To obtain lateral surfaces with various directions, we cut the sample using a FIB system with a gallium ion source. In this method, the single crystal was cut along planes with lower indices, such as the $(1,0,0)$ and $(0,0,1)$ planes, perpendicular to the conducting (a–c) plane in order to ensure the detection of the correct tunneling electrons corresponding to the cut surface direction. The sample crystal was glued by a silver paste on the sample holder of a glass plate. The current lead of a gold wire ($\phi = 50\,\mu m$) was attached to the sample with the silver paste. The sample holder was mounted with Apiezon N grease on the sample stage of an STM unit installed in a vacuum cell. We used a mechanically sharpened platinum–iridium wire as the STM tip. Prior to the STS measurement, we slowly cooled the sample at a rate of $\sim 0.5\,K/min$ around 80 K, because it is known that the volume fraction of the superconducting state decreases rapidly with increasing cooling rate for these materials.[19] The STS measurement was mainly carried out at 1.2 K, well below T_c, in a liquid helium bath by pumping with a mechanical vacuum pump. To avoid external vibration, the cryostat was mounted on a vibration isolator equipped with an air suspension system. The tunneling differential conductance dI/dV was directly obtained by lock-in detection, in which 500 Hz AC modulation with an amplitude of 0.2 mV was superposed on a ramped bias voltage with a period of 15 s.

3. Results and Discussion

3.1 STM observation of FIB-cut lateral surface

In order to check the surface condition, we performed STM measurement on both the as-grown and FIB-cut surfaces in the d[0,0]-Br salt at room temperature. Figure 1 shows STM images of the d[0,0]-Br salt on the as-grown [$(2,0,1)$ plane] and FIB-cut [$(1,0,0)$ plane] surfaces. In the STM image on the as-grown surface, we recognize the ET molecular array with the correct lattice spacing, denoted as the white arrows in Fig. 1(a). The present ET molecular image on the lateral surface of the d[0,0]-Br salt is similar to that of the $Cu(NCS)_2$ salt previously observed by other group.[20] In the image on the as-grown surface over a wider area ($600 \times 600\,nm^2$), the flat surface corresponding to the plane index $(2,0,1)$ spreads to the entire sample surface. This enables us to carry out angle-resolved STS. In the image on the FIB-cut surface, we also confirmed the ET molecular array in Fig. 1(b) with the correct lattice spacing as well as the as-grown surface. The flat surface with an area of about $70 \times 70\,nm^2$ corresponding to the $(1,0,0)$ plane spreads in the form of terraces. Therefore, it is considered that the tunneling electrons from both the as-grown and FIB-cut surfaces primarily reflect the surface direction, although other direction surface with a very small area is observed in the case of the FIB-cut surface.

3.2 In-plane anisotropy of the superconducting gap in κ-(ET-d[3,3])$_2$Cu[N(CN)$_2$]Br

Figure 2(a) shows the tunneling differential conductances dI/dV of the d[3,3]-Br salt obtained on the as-grown and

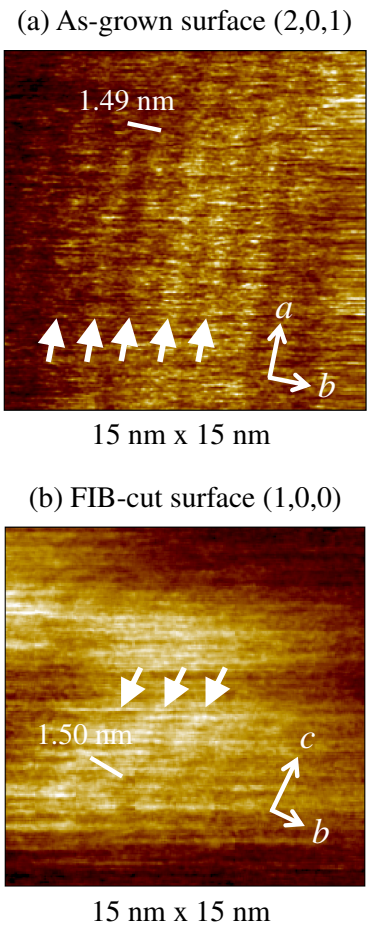

Fig. 1. (Color online) STM images of the d[0,0]-Br salt at room temperature. The white arrows indicate the ET molecular chain positions. (a) STM image on the as-grown surface of the $(2, 0, 1)$ plane. (b) STM image on the FIB-cut surface of the $(1, 0, 0)$ plane.

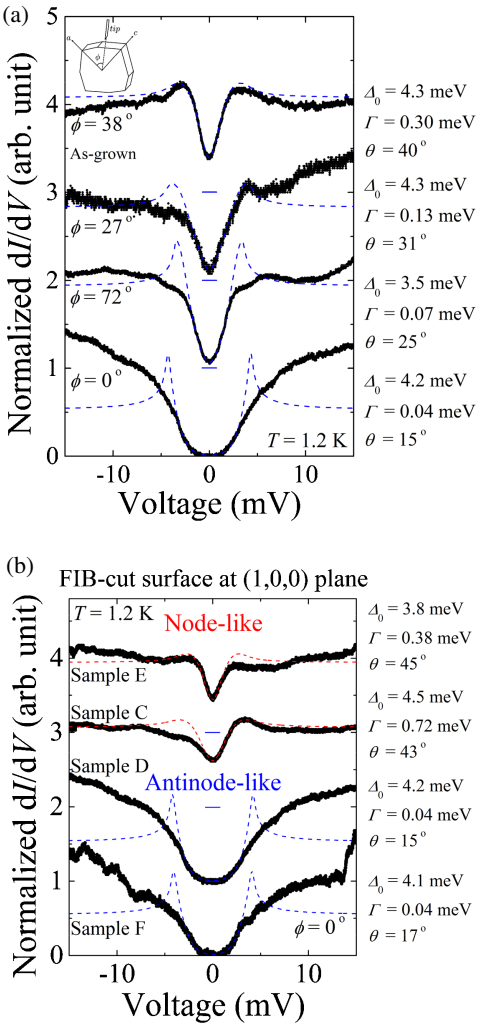

Fig. 2. (Color online) (a) Differential tunneling conductance dI/dV in κ-(ET-d[3,3])$_2$Cu[N(CN)$_2$]Br for surfaces of various angles. The parameter ϕ denotes the angle of the lateral surface from the a^*-axis in the a–c plane. Each curve is normalized by the conductance at $V = 10$ mV and aligned at intervals of one division for clarity. The broken line represents the curve calculated by the line nodes model. (b) Tunneling spectra on surfaces of the same angle at the $(1, 0, 0)$ plane in the d[3,3]-Br salt obtained by the FIB method. Two types of gap were observed on the surfaces of different samples with the same direction with high reproducibility. The broken line represents the curve calculated by the line nodes model.

FIB-cut lateral surfaces at 1.2 K. We adopted the highly reproducible data obtained by repeating tip approach on the same surface for the precise discussion of the STS results. It is considered that the differential conductance with high reproducibility is essential and reliable because this repeating tip approach corresponds to changing the tip position over a wider range than the distance between the ET molecules array, which is about 1.5 nm. To check the effect of the FIB method using gallium ions on the STS spectrum, we measured both the as-grown and FIB-cut surfaces at $(1, 0, 1)$ plane in the d[0,0]-Br salt. The STS spectrum on the FIB-cut surface was observed with high reproducibility, similarly to that of the as-grown surface. The observed tunneling spectra also had the same V-shaped form corresponding to the nodal direction with a comparable gap size. From these, it is considered that STS can be performed on the FIB-cut surface as well as on the as-grown surface without the effect of impurities such as gallium ions. The four curves obtained along the tunneling directions of $\phi = 0°$ (FIB), 72° (FIB), 27° (FIB), and 38° (as-grown), where ϕ is the azimuthal angle from the a^*-axis in the a–c plane as illustrated in the upper left of Fig. 2(a), are shown together. The plane indices corresponding to ϕ are estimated as $(2, 0, 1)$ at $\phi = 38°$, $(1, 0, 2)$ at $\phi = 72°$, $(3, 0, 1)$ at $\phi = 27°$, and $(1, 0, 0)$ at $\phi = 0°$. Each curve is normalized by the conductance at $V = 10$ mV and aligned at intervals of one division for clarity. Although dI/dV observed at $\phi = 0$ and 27° increases in the higher-energy region ($|V| > 5$ mV), probably due to the energy dependence of the tunneling probability, the functional form in lower-energy region, which correctly reflects the superconducting gap, is identical in each spectrum at surfaces of the same direction.

On the as-grown surface at $\phi = 38°$, we find a sharp dip in the lower-energy region associated with the superconducting gap. The value of dI/dV varies sharply around the lower-energy region depending on the bias voltage, and the dip associated with the superconducting gap is rather shallow at zero bias voltage. The observed V-shaped functional form of the gap indicates anisotropic superconductivity. On the FIB-cut surface at $\phi = 0$, 72, and 27°, we observed various gap forms, such as U-shaped and V-shaped gaps, depending on each FIB-cut surface direction. These gaps were observed

with high reproducibility for each surface for different tip approaches. In particular, the spectrum at $\phi = 0°$, which has the U-shaped functional form, had never been observed at an as-grown surface. It should be noted that we observed not only the U-shaped gap but also the V-shaped gap at the same FIB-cut surface of the $(1, 0, 0)$ plane with high reproducibility as shown in Fig. 2(b). In addition, a middle type gap, similar to the gap observed at $\phi \sim 36°$ [$(1, 0, 1)$ plane], was rarely observed in the case of the FIB-cut surface ($\phi = 0$ or 90°). However, the number of observations of the middle type gap was very small as compared with those of the above two types of gap. The middle type gap may have been caused by the exposure of another lower-plane-index surface, such as the $(1, 0, 1)$ plane, as a small area connecting the large flat area in the case of FIB-cut processing. Such a narrow area was also observed by STM measurement at room temperature, as described in the previous section. However, since most areas of the surface cut by FIB processing are almost flat, it is considered that the two types of superconducting gap observed with high reproducibility reflect the information from the correct plane. Therefore, we will proceed to a discussion without considering the middle type gap. For the moment, we adopt the U-shaped gap at $\phi = 0°$ in the angular dependence of the STS spectra in Fig. 2(a) by comprehensively considering the relationship between the form of each gap and its azimuthal angle ϕ. We discuss the two types of gap in a later section. It is strongly suggested from the systematic angular dependence of the STS spectra in Fig. 2(a) that the d[3,3]-Br salt is an anisotropic superconductor in the a–c plane, similarly to previously studied salts.

We try to fit each curve by the line nodes model considering the tunneling transition probability depending on the wave vector $\boldsymbol{k}$ of the tunneling electron, written as[11)]

$$\frac{dI}{dV} = G_{nn} \int \exp(-\beta \sin^2 \alpha) \int_{-\infty}^{\infty} N_s(E, \alpha) \times \left[-\frac{\partial f(E + eV)}{\partial (eV)} \right] dE \, d\alpha$$

with

$$N_s(E, \alpha) = N_0 \left(\mathrm{Re} \left[\frac{E - i\Gamma}{\sqrt{(E - i\Gamma)^2 - (\Delta_0 \cos 2(\alpha + \theta))^2}} \right] \right),$$

where Γ, G_{nn}, and θ are the electron lifetime broadening, the conductance of the sample at the normal state, and the fitting parameter which is the angle from the antinodal direction in the above model, respectively. The d-wave gap given as $\Delta = \Delta_0 \cos 2\theta$ is assumed. The material-dependent parameter β is fixed at $\beta = 15$. As shown in Fig. 2, all the observed curves are well fitted by the above model, as represented by the broken curves, especially in the lower-energy region, where the superconducting gap is correctly reflected. The obtained gap amplitudes Δ_0 on the FIB-cut surfaces are comparable to that on the as-grown surface ($\Delta_0 \sim 4.0$ meV). It is understood that each curve reflects the correct conductance corresponding to the surface direction. These facts additionally prove that the FIB method is effective for investigating the gap anisotropy in organic compounds in detail. As shown in Fig. 2(a), the superconducting gap varies systematically from the U-shaped antinodal form to the V-shaped nodal form with the fourfold symmetry of $\cos 2\theta$. This indicates that the d[3,3]-Br salt is a d-wave superconductor, similarly to the previously studied κ-ET salts.

3.3 *Strong-coupling d-wave superconductivity*

We estimate the gap parameter Δ_0 and $2\Delta_0/k_B T_c$ in the d[3,3]-Br salt as 4.0 ± 0.9 meV and 7.8 ± 1.8, respectively, from the results of angle-resolved STS on the lateral surface. These values for the d[3,3]-Br salt are comparable to those for the previously studied κ-ET salts ($\Delta_0 = 3.0$–10.0 meV, $2\Delta_0/k_B T_c = 6.7$–24.6 for the $Cu(NCS)_2$ salt; $\Delta_0 = 4.2 \pm 0.8$ meV, $2\Delta_0/k_B T_c = 8.1 \pm 1.5$ for the d[0,0]-Br salt; $\Delta_0 = 3.9 \pm 0.8$ meV, $2\Delta_0/k_B T_c = 7.6 \pm 1.5$ for the d[2,2]-Br salt). On the other hand, the value of $2\Delta_0/k_B T_c$ obtained from the results of STS on the lateral surface is slightly larger than that on the conducting plane ($\Delta_0 = 2.1 \pm 0.4$ meV, $2\Delta_0/k_B T_c = 4.1 \pm 0.7$ for the d[3,3]-Br salt). This tendency is common to all κ-ET salts. This discrepancy between the gap sizes obtained from the lateral surface and the conducting plane is presumably caused by the incomplete estimation of the gap amplitude on the conducting plane. Since Δ_0 is estimated from the average conductance curve in the d-wave line nodes model by assuming an isotropic 2D Fermi surface in the case of STS on the conducting plane, the influence of the in-plane anisotropy on the shape of the Fermi surface and the tunneling transition probability is not rigorously taken into account. The density of states probably has less weight along the a^*- and c^*-directions owing to the noncylindrical shape of the Fermi surface, and the group velocity component along the b^*-direction with the a^*- and c^*-axes corresponding to the tunneling probability may be small. As a result, the apparent gap size observed on the conducting plane is deduced to be smaller than the actual gap size. In contrast, we can directly obtain the superconducting gap in the case of STS on the lateral surface, which is less affected by the anisotropy of the Fermi surface. In fact, the gap sizes Δ_0 estimated from the STS for all directions ($\phi = 0$, 72, 27, and 38°) are comparable. Therefore, it is considered that the value obtained from the lateral surface reflects the correct gap size.

The value of $2\Delta_0/k_B T_c$ estimated from the lateral surface measurement in every salt is about twice that obtained by the mean field approximation ($2\Delta_0/k_B T_c = 4.28$) for weak-coupling with the d-wave.[21)] It is suggested that κ-ET salts including the d[3,3]-Br salt are strong-coupling d-wave superconductors, although a systematic change in $2\Delta_0/k_B T_c$ has not been confirmed within the experimental error with increasing electron correlation, which becomes stronger from the $Cu(NCS)_2$ salt to the d[3,3]-Br salt. The possibility of the strong-coupling d-wave superconductivity has also been discussed from the specific heat measurement of the d[0,0]-Br salt.[10)] The values of Δ_0 and $2\Delta_0/k_B T_c$ were estimated by the strong-coupling α-model as $\sim$3.8 meV and $\sim$7.4, respectively. These values are consistent with those obtained from the STS measurement.

3.4 *Nodal direction in κ-(ET-d[3,3])$_2$Cu[N(CN)$_2$]Br*

The relationship between the fitting parameter θ and the reduced azimuthal angle ϕ' is shown in Fig. 3 in order to determine the nodal direction. We deal with the azimuthal angle ϕ in the reduced range $0 \leq \phi' \leq \pi/4$ assuming the fourfold symmetry of $\Delta = \Delta_0 \cos 2\theta$ for simplicity because

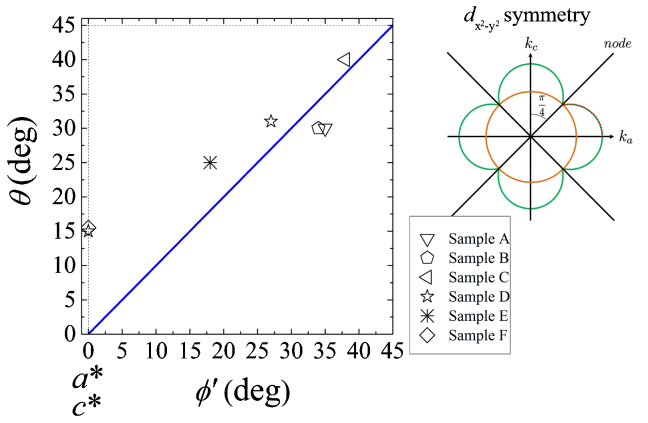

Fig. 3. (Color online) Relationship between the fitting parameter θ and the reduced azimuthal angle ϕ'. We adopt the data points of the U-shaped gap at $\phi' = 0°$ as written in the text. The solid line represents the relation for the $d_{x^2-y^2}$ symmetry. A schematic image of the $d_{x^2-y^2}$ symmetry is shown on the right side.

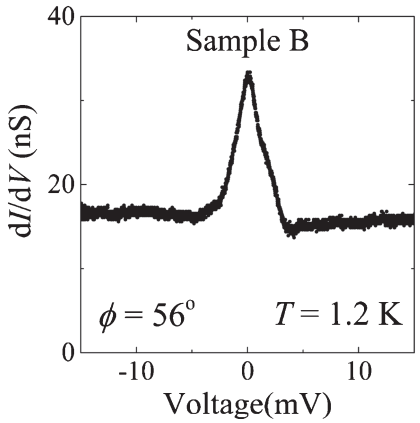

Fig. 4. Tunneling spectra of the zero bias conductance peak (ZBCP). The ZBCP was observed near the nodal direction corresponding to the $d_{x^2-y^2}$ symmetry.

the a^*-axis is perpendicular to the c^*-axis. For example, the direction of $\phi = 72°$ is reduced to $\phi' = 18°$. The data points of both the as-grown [(1, 0, 1), (2, 0, 1)] and FIB-cut surfaces are shown together, where the data with $\phi' > 35°$ and $\phi' < 35°$ correspond to the as-grown and FIB-cut surfaces, respectively. Here, we adopt the data of the U-shaped gap deduced from the entire tendency of the relationship between θ and ϕ', although two types of gap were observed at $\phi' = 0°$. We discuss the V-shaped gap observed at $\phi' = 0°$ in the next section. The plotted points almost lie on the solid line in Fig. 3. As a result, the nodal direction is determined to be $\pi/4$ from the a^*- and c^*-axes, and the symmetry of the superconductivity is $d_{x^2-y^2}$ as illustrated on the right side of Fig. 3. According to a theoretical study of the spin fluctuation mechanism,[12] this symmetry is stabilized in the case of a relatively weak electron correlation. Therefore, the electron correlation is still not strong enough even for the d[3,3]-Br salt in the framework of the spin fluctuation model, although the electron correlation of the d[3,3]-Br salt is stronger than those of the previously studied κ-ET salts.

In addition to the observation of the anisotropic gap, the ZBCP, which is a feature of anisotropic gapless superconductors with nodes, was also observed in the STS measurement on the lateral surfaces near the nodal direction, similarly to the d[0,0]-Br and d[2,2]-Br salts, when the STM tip was very close to the sample surface. As shown in Fig. 4, a sharp peak at zero bias was observed in the dI/dV curve. The observation of the ZBCP reinforces that the d[3,3]-Br salt is a d-wave superconductor with line nodes and is also consistent with the $d_{x^2-y^2}$ symmetry.

3.5 *Possibility of the coexistence of $d_{x^2-y^2}$ and d_{xy} symmetries*

Although we found that the symmetry of the superconductivity in the d[3,3]-Br salt is $d_{x^2-y^2}$, we also observed two types of superconducting gap, which are the nodal and antinodal gaps, at the same direction FIB-cut surface ($\phi = 0°$) as shown in Fig. 2(b). Only two types of gap were primarily observed at the same direction surface and other types of gap were hardly observed. As mentioned in Sect. 3.4, we adopted the U-shaped gap observed at the

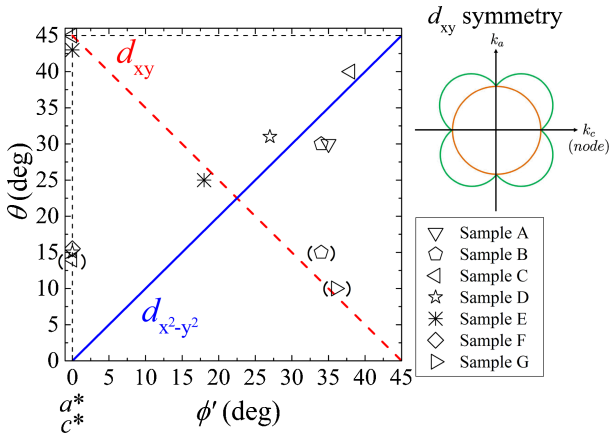

Fig. 5. (Color online) Relationship between the fitting parameter θ and the reduced azimuthal angle ϕ' containing the d_{xy} symmetry. The data points corresponding to another type of gap are added. The broken line represents the relation for the d_{xy} symmetry. A schematic image for the d_{xy} symmetry is shown on the right side.

FIB-cut surface ($\phi = 0°$) to determine the nodal direction in Fig. 3. However, the V-shaped gap is firmly observed. We add the corresponding data points at $\phi' = 0°$ to those in Fig. 3 around $\theta \sim 45°$ as shown in Fig. 5. Furthermore, we sometimes observed the two types of gap on the as-grown surface, although the reproducibility was not high. Such data points are also added as bracketed symbols such as (▷) at $\phi = 36°$, $\theta = 10°$ in Fig. 5. These data points do not correspond to the solid line representing the $d_{x^2-y^2}$ symmetry. Instead, these additional points are aligned on another linear relation shown as the broken line in Fig. 5 indicating the d_{xy} symmetry. These two types of gap have never been observed in the d[0,0]-Br or Cu(NCS)$_2$ salts. It is known that the d[3,3]-Br salt has an antiferromagnetic insulating region in part at the superconducting state even if the sample is cooled slowly around 80 K. In this measurement, since we cooled the sample at a rate of ~0.5 K/min around 80 K, it is presumed that the volume fraction of the superconducting state is about half of the entire sample volume in accordance with previous research.[19] Such a mosaic pattern is sketched in Fig. 6, although the detailed spatial structure is not yet

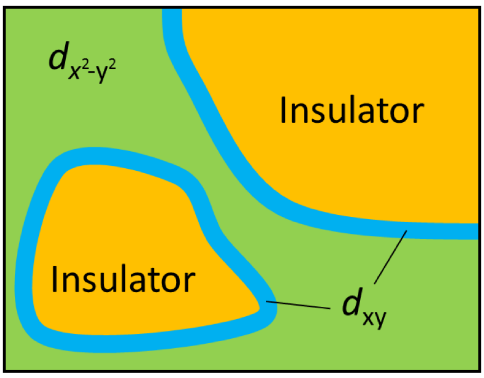

Fig. 6. (Color online) Schematic image of the coexistence of the $d_{x^2-y^2}$ and d_{xy} symmetries. The $d_{x^2-y^2}$ symmetry is stabilized in the bulk superconducting phase, while the d_{xy} symmetry appears around the antiferromagnetic insulating region.

known. The $d_{x^2-y^2}$ symmetry is stabilized in the bulk superconducting region, where the electron correlation is not strong enough. On the other hand, it is presumed that the electron correlation becomes stronger locally around the insulating region. Therefore, the nodal gap at $\phi = 0°$ corresponding to the d_{xy} symmetry could be observed near the insulating region as shown in Fig. 6. The observation of two types of gap suggests the possibility of the coexistence of the $d_{x^2-y^2}$ and d_{xy} symmetries. This behavior probably corresponds to the change from the $d_{x^2-y^2}$ to d_{xy} symmetries with increasing electron correlation predicted by the spin fluctuation model. It presumably indicates that the mechanism of the superconductivity in κ-ET salts is caused by the antiferromagnetic spin fluctuation.

4. Conclusion

We performed angle-resolved STS measurement on as-grown and FIB-cut lateral surfaces of κ-(ET-d[3,3])$_2$Cu[N(CN)$_2$]Br to clarify the mechanism of its superconductivity. We succeeded to observe the systematic in-plane anisotropy of the superconducting gap depending on the tunneling direction. As a result, we found that the superconducting gap in the d[3,3]-Br salt is a strong-coupling d-wave superconductor. We also manifested that the FIB method is useful to investigate the in-plane superconducting gap anisotropy in organic compounds which have no cleavage. The gap symmetry is described by $d_{x^2-y^2}$ in the bulk superconducting phase, similarly to the previously studied κ-ET salts. This suggests that the electron correlation in the d[3,3]-Br salt is still not strong enough in the framework of the spin fluctuation model, although the electron correlation in the d[3,3]-Br salt, which is situated very near the Mott boundary, is stronger than that in the previously studied κ-ET salts.

In addition, we also observed two types of superconducting gap at the same direction surfaces. This suggests the possibility of the coexistence of regions with the $d_{x^2-y^2}$ and d_{xy} symmetries. This behavior probably corresponds to the change from the $d_{x^2-y^2}$ to d_{xy} symmetries with increasing electron correlation predicted by the spin fluctuation model.

Acknowledgments

We are grateful to S. Tanda for his kind permission to use the FIB apparatus. This study was supported in part by a Grant-in-Aid for Science Research (Grant No. 25610083) from the Ministry of Education, Culture, Sports, Science and Technology.

1) K. Kanoda, Hyperfine Interactions **104**, 235 (1997).
2) Y. Tokura, Kotai Butsuri **28**, 557 (1993) [in Japanese].
3) U. Geiser, A. J. Schultz, H. H. Wang, D. M. Watkins, D. L. Stupka, J. M. Williams, J. E. Schiber, D. L. Overmyer, D. Jung, J. J. Novoa, and M.-H. Whango, Physica C **174**, 475 (1991).
4) A. Kawamoto, H. Taniguchi, and K. Kanoda, J. Am. Chem. Soc. **120**, 10984 (1998).
5) A. Kawamoto, K. Miyagawa, and K. Kanoda, Phys. Rev. B **55**, 14140 (1997).
6) G. Saito, H. Yamochi, T. Nakamura, T. Komatsu, T. Ishiguro, Y. Nogami, Y. Ito, H. Mori, K. Oshima, M. Nakashima, S. Uchida, H. Takagi, S. Kagoshima, and T. Osada, Synth. Met. **42**, 1993 (1991).
7) S. M. De Soto, C. P. Slichter, A. M. Kini, H. H. Wang, U. Geiser, and J. M. Williams, Phys. Rev. B **52**, 10364 (1995).
8) H. Mayaffre, P. Wzietek, D. Jerome, C. Lenoir, and P. Batail, Phys. Rev. Lett. **75**, 4122 (1995).
9) Y. Nakazawa and K. Kanoda, Phys. Rev. B **55**, R8670 (1997).
10) O. J. Taylor, A. Carrington, and J. A. Schlueter, Phys. Rev. Lett. **99**, 057001 (2007).
11) T. Arai, K. Ichimura, K. Nomura, S. Takasaki, J. Yamada, S. Nakatsuji, and H. Anzai, Phys. Rev. B **63**, 104518 (2001).
12) K. Kuroki, T. Kimura, R. Arita, Y. Tanaka, and Y. Matsuda, Phys. Rev. B **65**, 100516 (2002).
13) K. Ichimura, M. Takami, and K. Nomura, J. Phys. Soc. Jpn. **77**, 114707 (2008).
14) Y. Oka, R. Abe, H. Nobukane, N. Matsunaga, K. Nomura, K. Ichimura, and A. Kawamoto, J. Phys.: Conf. Ser. **400**, 022090 (2012).
15) S. Kashiwaya and Y. Tanaka, Rep. Prog. Phys. **63**, 1641 (2000).
16) K. Suzuki, K. Ichimura, K. Nomura, and S. Takekawa, J. Phys.: Condens. Matter **11**, 3133 (1999).
17) S. Tanaka, E. Ueda, M. Sato, K. Tamasaku, and S. Uchida, J. Phys. Soc. Jpn. **64**, 1476 (1995).
18) H. Anzai, M. J. Delrieu, S. Takasaki, S. Nakatsuji, and J. Yamada, J. Cryst. Growth **154**, 145 (1995).
19) H. Taniguchi, A. Kawamoto, and K. Kanoda, Phys. Rev. B **59**, 8424 (1999).
20) M. Yoshimura, H. Shigekawa, H. Nejoh, G. Saito, Y. Saito, and A. Kawazu, Phys. Rev. B **43**, 13590 (1991).
21) H. Won and K. Maki, Phys. Rev. B **49**, 1397 (1994).